Dependency of Cyclic Plastic Deformation Characteristics of Unsaturated Recycled Base Course Material on Principal Stress Axis Rotation

A. Inam[1], T. Ishikawa[2], and S. Miura[3]
[1]*Deputy Director (HRTC), National Highway Authority, Ministry of Communications, Pakistan*
[2]*Associate Professor, Graduate School of Engineering, Hokkaido University, Japan*
[3]*Professor, Graduate School of Engineering, Hokkaido University, Japan*
E-mail: aasiminam@yahoo.com

ABSTRACT: Nowadays, in order to economize the cost of pavements, recycled crusher-run (recycled concrete) that is recycled material is employed as base course material instead of natural crusher-run (andesite). Therefore, mechanical response of recycled crusher-run is required to evaluate in order to construct quality roads with minimum cost. In this research paper, an attempt is made to determine strength-deformation characteristics of unsaturated recycled crusher-run material, under various loading conditions and saturation degrees. In addition, cyclic plastic deformation behaviour of two types of materials that are natural crusher-run (andesite) and recycled crusher-run (recycled concrete) is compared and analysed. A series of laboratory element test were carried out by using multi-ring shear apparatus, which can take in to account the rotation of principal stress axis. The experimental results show that, cyclic plastic deformation considerably enhances due to the rotation of principal stress axis under repeated axial and shear loading tests. Moreover, cyclic plastic deformation of recycled crusher-run material increases to some extent when compared with natural crusher-run material under same experimental conditions.

1. INTRODUCTION

The main function of the base course in pavement structure is to provide structural support to top layer of the pavement. In Japan, the natural crusher-run material (granular material) is employed as base course for pavement subject to fulfilling the material properties as described in the specifications. The subbase is an optional layer. It is normally placed over subgrade, when the suitable material for the base course is either not locally available or quite expensive and/or subgrade soil is of very poor quality. It is made up of economical material with relatively low load bearing capacity compared to the base course materials. Therefore, the inclusion of a subbase course is primarily an economic issue. Natural crusher-run material can be used as subbase material, if it fulfills the criteria to achieve the economy and conform the subbase material properties as described in the specifications by Japan Road Association (1989). The significant increase in the construction, rehabilitation and maintenance of highways continuously enhances the demand of pavement construction materials. After completing the service life of infrastructure, such as highways and buildings, disposal of construction material is also one of the environmental concerns. Therefore, the recycled crusher-run material made from construction waste (recycled concrete) is also used in base course for common roads. According to pavement design manual issued by Japan Road Association (2006), traffic volume for the common road is less than 100 vehicle pass/day/direction and it comes under the category of N1, N2 and N3. Where, N1 has the traffic volume less than 15 vehicle pass/day/direction, N2 ranges from 15 to less than 40 vehicle pass/ day/direction and N3 ranges from 40 to less than 100 vehicle pass/day/direction. The laying of the recycled crusher-run material as base course can save huge cost on pavement construction, solve disposal issue of construction material and decrease the usage of natural crusher-run material. However, prior to employ the recycled crusher-run material in a base course, strength-deformation characteristics are needed to study under traffic loads. It is pertinent to mention that the recycled crusher-run material can be used in the base course, when the mechanical and physical properties of recycled material meet the standards and specifications of highways. It has been found that plenty of work has been carried out in order to establish specifications and to examine the properties and usages of recycled concrete aggregate in construction industry such as Kobayashi and Kawano (1988), Poon and Chan (2006) and Gabr and Cameron (2012). This research could be helpful to resolve the cyclic plastic deformation behavior of the unsaturated recycled crusher-run employed as base course material under traffic loads.

Water can penetrate into pavement structures through various means. It is not possible to completely restrict the penetration of water in to pavement layers. However, the drainage system for pavements is designed and constructed in such a way that the minimum water should be infiltrated into the pavement layers in order to keep pavement unsaturated. In general, asphalt surface mixtures act as water proof layer and prevent rain water from penetrating into the pavement. Such type of surface mixtures facilitate the discharging of surface water through cross-slope having 1.5 to 2.0 % gradient. In addition to above, drainage asphalt pavement is used in Japan. In drainage asphalt pavement, open grade friction course also known as porous friction course is used as surface course. One of the purposes of the surface course is to provide drainage layer that permits surface water to migrate laterally through the mixture to the edge of the pavement. The drainage mechanism in two types of surface mixtures is shown in Figure 1. It is pertinent to mention that one of the reasons for deterioration of the pavement is infiltration of water into the base course. This infiltration and seasonal variations of groundwater level cause fluctuation in degree of saturation S_r inside the base course throughout a year. Therefore, in the pavement designing and construction, the water content is an important attribute to influence the strength-deformation characteristic of base course. Accordingly, in this research, main focus is on the mechanical behavior of unsaturated base course consisted of recycled crusher-run material under traffic load.

Besides the significance of understanding the behavior of the unsaturated granular base course consisted of recycled crusher-run material, an appropriate loading method for laboratory element tests is also critical for pavement design and analysis. It is noted in various research works that the behavior of pavement structure under traffic loads differs from that in laboratory tests, such as repeated axial loading test. The main difference is due to the rotation of principal stress axis. The outcomes of laboratory element tests, in which principal stress axis rotation is applied, represents more reliable deformation behavior of granular material, and its importance to the performance of pavement and rail-road track has been mentioned by various researchers (Chan and Brown 1994, Brown 1996 and Gräbe and Clayton 2009). In addition, laboratory element test, such as triaxial compression test, generally employs axial compression loading without principal stress axis rotation.

Consequently the phenomenon of principal stress axis rotation has not been reproduced concisely by the conventional testing methods.

Keeping in view the aforementioned, Ishikawa et al. (2007) developed multi-ring shear apparatus for laboratory element tests. The multi-ring shear apparatus employed in this research can take into account rotation of principal stress axis like in-situ conditions and is used to evaluate strength-deformation characteristics of granular base course material. In previous research (Inam et al. 2012), an effort was made to describe the deformation behavior of unsaturated natural crusher-run material used in the base course by employing multi-ring shear testing apparatus. In this research, recycled crusher-run is used to determine strength-deformation characteristics of unsaturated base course under the influence of principal stress axis rotation, which was not examined in the previous research. The same experimental conditions as applied in the previous research are adopted for recycled crusher-run in this research, which is necessary in order to compare strength-deformation characteristics of recycled crusher-run with natural crusher-run. The comparisons and differences in the results of two types of materials discussed on the scientific and analytical basis are the reasons / causes to establish the originality of this research paper. In consequence of comparison of two types of materials, new findings and conclusions are observed. Keeping in foregoing, this research brings new insight into the unsaturated behavior of base course materials.

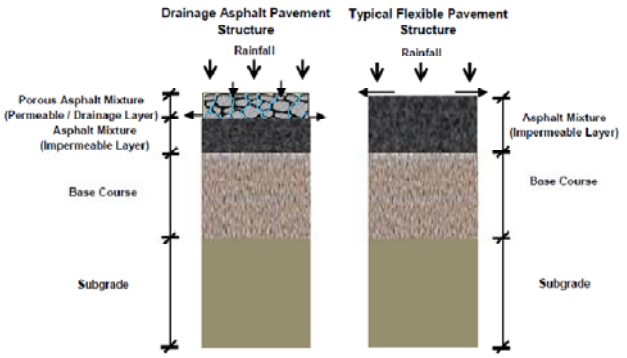

Figure 1 Drainage mechanism in two types of surface mixtures

2. TEST MATERIAL

2.1 Physical Properties

The C-40 (Natural crusher-run which has maximum particle size of 40 mm) is used in Japanese roads as the base course material; it is composed of angular, crush, hard andesite stone. The grading of C-40 means, it has a grain size distribution between 0 mm and 40 mm. RCA-40 (Recycled crusher-run which has also maximum particle size of 40 mm) with similar particle size distribution to that of C-40 is adopted in this research. The recycled crusher-run material is obtained from demolished concrete structure. In multi-ring shear apparatus width of specimen is 60 mm. In this research maximum particle size was selected 9.5 mm because according to the standard test method for determining the resilient modulus of soils and aggregate materials (AASHTO T 307-99 (2007) 2009), minimum diameter of the mold sizes to fabricate specimens should be equal or greater than five times the maximum particle size. Therefore, in this research recycled crusher-run material which has the maximum particle size of 9.5 mm (RCA-9.5) was selected for multi-ring shear tests. RCA-9.5 material is about one fourth of the mean particle size of original RCA-40. The scale down of gradation may influence the behavior of the material on the permeability and void ratios due to change in the ratio of coarser to finer particles. However, scale down effect of gradation on cyclic plastic deformation behavior is not considered in this research, since the effect of scale down of material in the experimental program could not be studied due to limitation of width of specimen used in multi-ring shear testing. Emphasis is made to examine the cyclic plastic deformation characteristics under the influence of principal stress axis rotation, though there is a room for further research to investigate the influence of the scale down effect of gradation from maximum particle size of 40 mm to 9.5 mm on cyclic plastic deformation characteristics of unsaturated base course material under different loading methods. RCA-9.5 material is prepared by screening out particles larger than 9.5 mm from RCA-40 material and washing inside a 0.075 mm sieve. The process of washing inside sieve was carried out in order to remove fine particles because fine particles can enter between small gaps of rings of multi-ring shear apparatus. After washing, RCA-9.5 material is dried in oven for 24 hours at least. Physical properties of C-9.5 (Natural crusher-run material which has the maximum particle size of 9.5 mm employed in Inam et al. 2012), C-40, RCA-9.5 and RCA-40 materials are described in Table 1. Particle size distribution curves of C-9.5, C-40, RCA-9.5 and RCA-40 materials are shown in Figure 2.

Table 1 Physical Properties of Test Materials

Name of material	Average diameter, D_{50} (mm)	Specific gravity, G_s	Water absorption (%)	Los Angeles abrasion value (%)
C-9.5	2.7	2.753	4.3	-
C-40	10.8	2.737	3.7	18.8
RCA-9.5	2.8	2.712	8.4	-
RCA-40	10.8	2.686	6.6	24.5

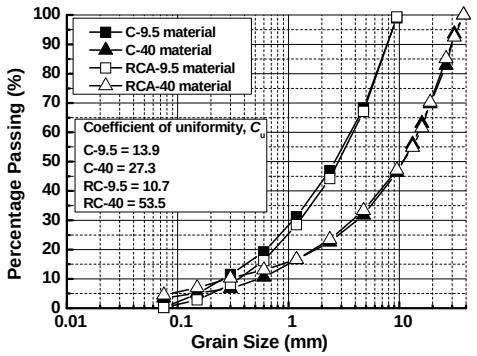

Figure 2 Particle size distribution curves for test materials

2.2 Moisture - density relationship

The compaction curve of RCA-9.5 material was determined by A-b method of Japanese industrial standard (Japan Standards Association 2009). In this method, a mold diameter of 100 mm, a mold height of 127 mm and a drop height of 300 mm for the rammer are used. The test material is compacted in three equal layers by applying 25 blows to each layer with a 2.5 kg rammer to obtain the compaction energy E_c of 550 kJ/m^3. The moisture-density curve for the RCA-9.5 material with the optimum moisture content w_{opt} of 13.8 % and the maximum dry density ρ_{dmax} of 1.650 g/cm^3 is shown in Figure 3. The moisture-density curve for C-9.5 material with the w_{opt} of 9.5 % and the ρ_{dmax} of 1.775 g/cm^3 is obtained from previous research (Inam et al. 2012) by applying same method as mentioned above.

2.3 Soil water characteristic curve

In accordance with standards by Japan Geotechnical Society (2009), water retentivity test on RCA-9.5 material was carried out by using triaxial apparatus to determine the soil water characteristic curve (SWCC) of unsaturated soils. It has been found that not many studies were carried out to determine the SWCC for coarse grained material. The quite possible reason is that lower matric suction *s*

occurs in case of coarse grained material as compared to fine grained and cohesive soils (Ekblad and Isacsson 2006). ASTM designation 6836-02 (2010) is the standard testing method of the soil water characteristic curve for desorption by using a Hanging Column, Pressure Extractor, Chilled Mirror Hygrometer, and/or Centrifuge.

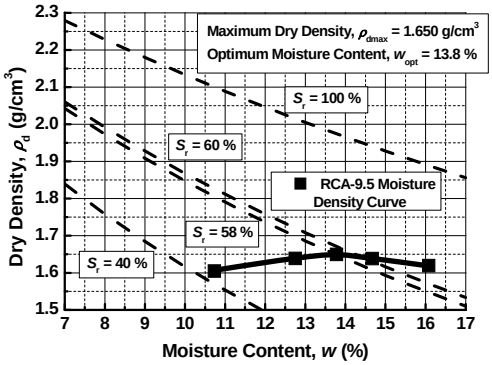

Figure 3 Moisture-density curve for RCA-9.5 material

The multi-ring shear apparatus cannot measure or control the s, therefore, triaxial apparatus developed by Ishikawa et al. (2010) for unsaturated soils that adopt the pressure membrane method to determine soil water characteristic curve is employed in this research. The RCA-9.5 specimen (170 mm in height and 70 mm in diameter) was prepared in the triaxial apparatus so that dry density after consolidation ρ_{dc} became 1.470 g/cm^3, which was the same dry density ρ_d before conducting multi-ring shear tests in this research. The triaxial apparatus can control pore air pressure u_a and pore water pressure u_w at the cap and the pedestal, separately. The u_w is applied through a hydrophilic versa pore membrane filter attached to the water plumbing path, and the u_a is applied through a hydrophobic polyflon filter attached to the air supply path. The validity of using these filters was examined by Ishikawa et al. (2010).

The air-entry value is defined by Rahardjo et al. (2011) that the s value at which air first enters the pores of the soil. It is indication of s at which water in large pores started to drain and beyond the air-entry value, desaturation occurs rapidly. It has been found that air-entry value for the SWCC in this research is not clearly recognized at low suction ranges or in other words s has such a small value at air-entry value that cannot be noticed or recognized while performing water retentivity test on triaxial apparatus. Ishikawa et al. (2012b) described similar behavior that air-entry value could not be found on coarse material such as C-40. During isotropic consolidation, net confining pressure $\sigma_{c(net)}$ of 49 kPa was applied on RCA-9.5 material in order to achieve the desire ρ_d. The net confining pressure is defined as $\sigma_{c(net)} = \sigma_c - u_a$. Figure 4 shows the results of water retentivity test on RCA-9.5 material in comparison with SWCC for C-9.5 material at 1.580 g/cm^3 of ρ_{dc} obtained from previous research (Inam et al. 2012).

The experimental conditions to carry out water retentivity test of RCA-9.5 and C-9.5 materials are described in Table 2. The ρ_d of C-9.5 and RCA-9.5 is taken at about 90 % of degree of compaction D_c though initial void ratio e_0 for RCA-9.5 is 0.85 and for C-9.5 is 0.74 as shown in Table 2. The SWCC shows the relationship between the s and the S_r. The s can be defined as the difference between u_a and u_w acting on the contractile skin (Fredlund and Rahardjo 1993). In Figure 4, drying curve for RCA-9.5 material shows that S_{r0} is about 25.0 % and drying curve for C-9.5 material shows that S_{r0} is about 11.0 %. The S_{ro} is defined by many researchers. According to Rahardjo et al. (2011) and Fredlund and Xing (1994), the residual water content is the water content where a large suction change is required to remove additional water from soil or in other words residual water content is the state where the S_r of a soil experiences no significant change with the s increases. The S_{r0} obtained in the SWCC of RCA-9.5 and C-9.5 materials are much lower than the S_r at the w_{opt} as indicated in Figure 3 and Inam et al. (2012) respectively. Ishikawa et al. (2012a) shows that based on their long-term field measurement full scale test pavement, the S_r inside sub-base course (C-40 material) is a little higher than 30 % during most of the time in a year. In addition, the result of water retentivity test on C-40 material with 95 % of D_c also shows that the S_{r0} is little higher than 30 % (Ishikawa et al. 2012b). Besides, it is found that the S_r of C-40 material at the w_{opt} of 8.2 % is about 55 %. These show that during most of the time in a year, the S_r inside real sub-base course is much lower than the S_r at the w_{opt} and such S_r inside real sub-base course can be better expressed by the S_{r0} obtained through water retentivity tests. On the other hand, it was described in previous research (Inam et al. 2012), that the s of samples with S_r = 19 % (moisture content w = 5 %), 33 % (w = 9 %) and 48 % (w = 13 %) has an insignificant influence on shear behavior of C-9.5 material due to low s values as shown in the drying curve of Figure 4. In case of RCA-9.5 material, low s values occur under different S_r and, as a result, insignificant influence of s on the shear behavior will also be observed in this research. The insignificant influence of s on the shear behavior for RCA-9.5 material is explained in latter section.

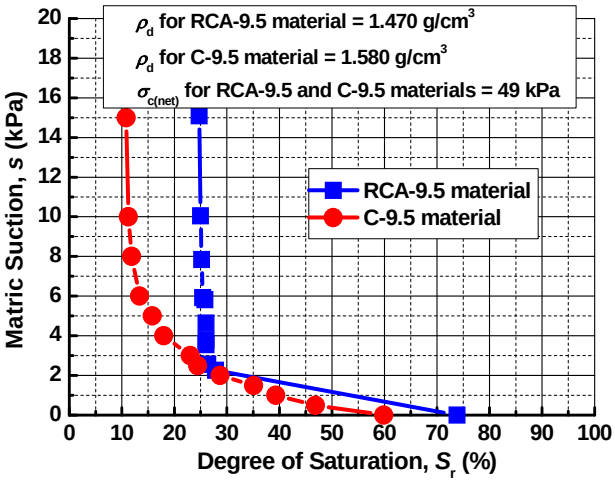

Figure 4 Soil water characteristic curves for RCA-9.5 and C-9.5 from Inam et al. (2012)

Table 2 Experimental Conditions for Water Retentivity Test

Name of material	Dry density, ρ_d, (g/cm^3)	Degree of compaction, D_c (%)	Initial void ratio, e_0
RCA-9.5	1.470	90	0.85
C-9.5	1.580	90	0.74

3. TESTING METHOD

A schematic diagram of multi-ring shear and the components of multi-ring shear apparatus were explained by Inam et al. (2012). The terms regarding size, load, stress, strain and axis used in multi-ring shear tests was also described in Inam et al. (2012). The width of specimen is 60 mm (120 mm inside diameter and 240 mm outside diameter) and the height is 60 mm.

3.1 Experimental Conditions

A series of static and cyclic loading tests were performed with the multi-ring shear apparatus. The criteria to determine experimental conditions for RCA-9.5 material described here were taken from previous research (Inam et al. 2012) in order to compare deformation behavior of RCA-9.5 material with C-9.5 material. Therefore, S_r of 19 %, 33 % and 48 % were selected for RCA-9.5

unsaturated specimens. The S_r of 19 % is lower than the S_{r0} of RCA-9.5 material as shown in Figure 4. The S_{r0} is not the lowest possible S_r within soil and it is possible for the water content to be less than the residual water content through evaporation, centrifuging or even the drying as defined by Vanapalli et al. (1998). The prescribed water content is added to the oven-dried RCA-9.5 material. The oven-dried sample was also selected to compare the results with those of the unsaturated specimen's results. Afterwards, the RCA-9.5 material is placed in three equal layers over the bottom plate, confined by outer and inner rigid rings and compacted uniformly to achieve desired ρ_d.

In accordance with the Japanese highway standards, a ρ_{dmax} of 95 % is commonly taken in the field conditions. However, due to the limitation of multi-ring shear apparatus, 95 % of the ρ_{dmax} could not be achieved for the C-9.5 material (Inam et al. 2012); therefore, for C-9.5 material about 90 % of the ρ_{dmax} (ρ_{dmax} = 1.775 g/cm^3) was selected in previous research (Inam et al. 2012). Likewise, for the RCA-9.5 material, a ρ_d of 1.470 g/cm^3 was selected for the multi-ring shear test which is also about 90 % of the ρ_{dmax} (ρ_{dmax} = 1.650 g/cm^3 as shown in Figure 3).

In this research same stress distributions are considered in the multi-ring shear tests for the RCA-9.5 material which was adopted in previous research (Inam et al. 2012) for the C-9.5 material in order to compare strength-deformation characteristics. The axial stress and the shear stress distribution are shown in Figure 5 and the loading frequency of 0.02 Hz was taken for the cyclic loading tests of RCA-9.5 material. After preparing the sample, static and cyclic loading tests were performed on the RCA-9.5 material to examine the mechanical behavior of recycled base course material under different S_r by using the multi-ring shear apparatus. In the case of the static test on RCA-9.5 material, shear stress $\tau_{a\theta}$ was monotonically increased at the rate of shear strain $\gamma_{a\theta}$ of 0.1 %/min while keeping constant axial stress σ_a of 114.2 kPa. In the cyclic loading tests two loading modes were implemented to evaluate the cyclic deformation characteristics of unsaturated specimen. One mode is the cyclic axial loading, which is considered as repeated axial loading without rotation of the principal stress axis. In this method, only the axial load in the sinusoidal waveform is cyclically applied to the specimen and maximum axial stress σ_{amax} is taken as 114.2 kPa. Hereafter, cyclic axial test without principal stress axis rotation will be referred to as repeated axial loading test. The other mode is the cyclic axial and shear loading, in which the axial load and the shear load, both in the sinusoidal waveform are cyclically applied to the specimen. The shear load is cyclically applied for bidirectional loading, similar to two-way traffic on pavement by changing phase angle of 180 degrees for every succeeding loading cycle (Inam et al. 2012). Hereafter, cyclic axial and shear loading tests will be referred to as repeated axial and shear loading test similar to in-situ traffic loading conditions, in which the rotation of principal stress axis occurs.

In repeated axial and shear loading tests the σ_{amax} of 114.2 kPa and the maximum shear stress $\tau_{a\theta max}$ of 30 kPa were considered as shown in Figure 5. The stress paths between the mean principal stress $p = (\sigma_1 + \sigma_2 + \sigma_3)/3$ and the deviatoric stress $q = (\sigma_1 - \sigma_3)$ for the cyclic loading tests at the coefficient of earth pressure at rest K_0 = 0.30 (K_0 value is taken as an example) are shown in Figure 6. The principal stresses values σ_1, σ_2, σ_3 and K_0 value for the cyclic loading tests were estimated and described in latter section. The experimental conditions for the multi-ring shear tests performed in this research are summarized in Table 3.

4.1 Influence of degree of saturation on shear behavior

The results of static shearing tests for the RCA-9.5 material are presented in Figures 7-13 showing the relationships among $\gamma_{a\theta}$, $\tau_{a\theta}$ and axial strain ε_a under different S_r. Figures 7 and 8, clearly show that increase in the $\tau_{a\theta}$ on each curve causes increase in the ε_a and in the $\gamma_{a\theta}$ on the same curve. However, when comparing any two curves obtained from the static shearing test under different S_r, the following trends can be seen as a general shear behavior as shown in Figures 9 to 11.

- $\tau_{a\theta}$ is inversely proportional to a ε_a at the same $\gamma_{a\theta}$.
- $\tau_{a\theta}$ is directly proportional to $\gamma_{a\theta}$ at the same ε_a.
- $\gamma_{a\theta}$ is directly proportional to ε_a at the same $\tau_{a\theta}$.

4. RESULTS AND DISCUSSIONS

Figure 12 shows the relationships between S_r - $\gamma_{a\theta}$ and S_r - ε_a at the $\tau_{a\theta}$ of 30 kPa. It is further elaborated that an oven-dried sample has the minimum shear strain $\gamma_{a\theta min}$ and the minimum axial strain ε_{amin} at the $\tau_{a\theta}$ of 30 kPa. The graph also shows that the sample with S_r = 19 % has the maximum shear strain $\gamma_{a\theta max}$ and the maximum axial strain ε_{amax} at the $\tau_{a\theta}$ of 30 kPa. The decreasing sequence of the ε_a and the $\gamma_{a\theta}$ under the constant $\tau_{a\theta}$ of 30 kPa is S_r = 19 %, S_r = 33 %, S_r = 48 % and finally oven-dried (S_r = 0 %)

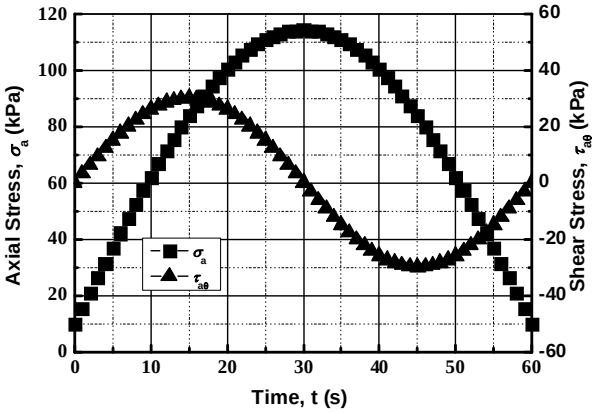

Figure 5 Cyclic loading pattern in multi-ring shear tests (Inam et al. 2012)

Table 3 Experimental Conditions for Multi-ring Shear Tests

(a) Static Shearing Tests on RCA-9.5 Material

Degree of saturation, S_r (%)	Oven-dried, 19, 33 & 48
Initial dry density, ρ_{d0} (g/cm^3)	1.450
Dry density after consolidation, ρ_{dc} (g/cm^3)	1.470
Constant axial stress, σ_a (kPa)	114.2

(b) Repeated Axial Loading Tests on RCA-9.5 Material

Degree of saturation, S_r (%)	Oven-dried, 19, 33 & 48
Dry density before test, ρ_{d0} (g/cm^3)	1.470
Axial stress, σ_{amax} (kPa)	114.2
Loading frequency (Hz)	0.02
Number of loading cycles, N_c	400

(c) Repeated Axial and Shear Loading Tests on RCA-9.5 Material

Degree of saturation, S_r (%)	Oven-dried, 19, 33 & 48
Dry density before test, ρ_{d0} (g/cm^3)	1.470
Axial stress, σ_{amax} (kPa)	114.2
Shear stress, $\tau_{a\theta max}$ (kPa)	30
Loading frequency (Hz)	0.02
Number of loading cycles, N_c	400

During static shearing tests, shear loading was applied up to the $\gamma_{a\theta}$ of 3.0 % for the RCA-9.5 material. The $\gamma_{a\theta}$ of 3.0 % was selected for the RCA-9.5 because in previous research the $\gamma_{a\theta}$ of 3.0 % was taken for the C-9.5 material due to the limitation of torque transducer installed in the multi-ring shear apparatus. On this basis, the $\tau_{a\theta}$ and the ε_a behavior were analyzed under different S_r at the $\gamma_{a\theta}$ of 3.0 % as shown in Figure 13. It is seen that the oven-dried sample has the ε_{amin} and the $\tau_{a\theta max}$ at the $\gamma_{a\theta}$ of 3.0 %. On the other hand, the sample with a S_r = 19 % has the ε_{amax} and the minimum shear stress $\tau_{a\theta min}$ at the $\gamma_{a\theta}$ of 3.0 %. The sequence for the increase in $\tau_{a\theta}$ and the decrease in ε_a at the $\gamma_{a\theta}$ of 3.0 % under different S_r is the same as mentioned in above paragraph. It was found that there is no breakage of the particles or changes in particle size distribution before and after testing.

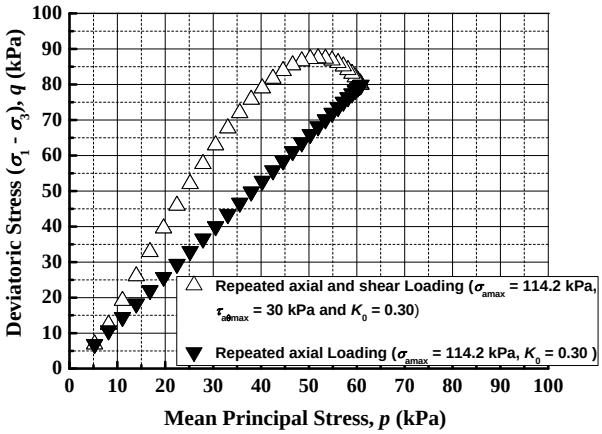

Figure 6 Stress paths for cyclic loading test

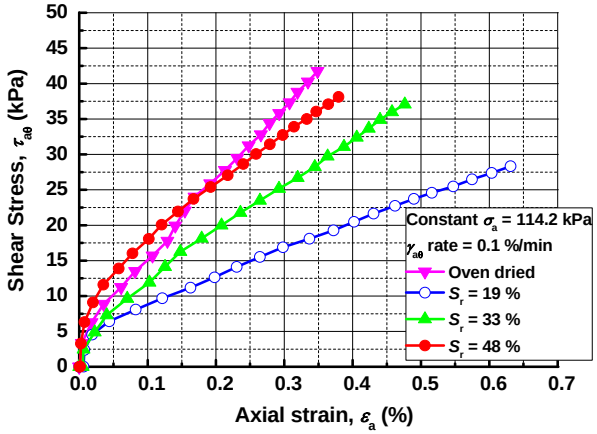

Figure 7 ε_a - $\tau_{a\theta}$ relationships under static shearing test (RCA-9.5)

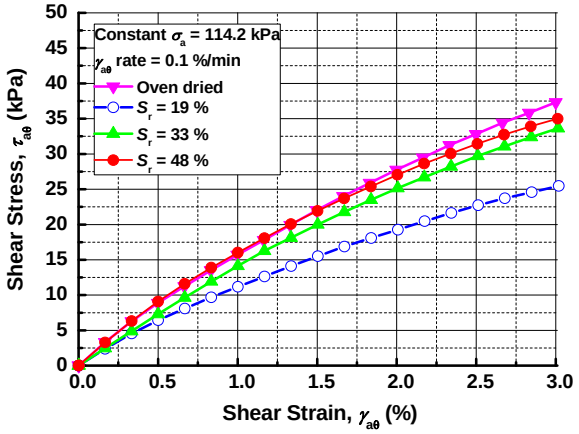

Figure 8 $\gamma_{a\theta}$ - $\tau_{a\theta}$ relationships under static shearing test (RCA-9.5)

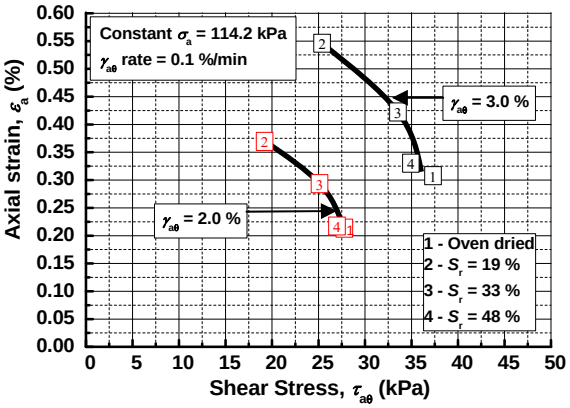

Figure 9 $\tau_{a\theta}$ - ε_a relationships during static shearing test at the same $\gamma_{a\theta}$ (RCA-9.5)

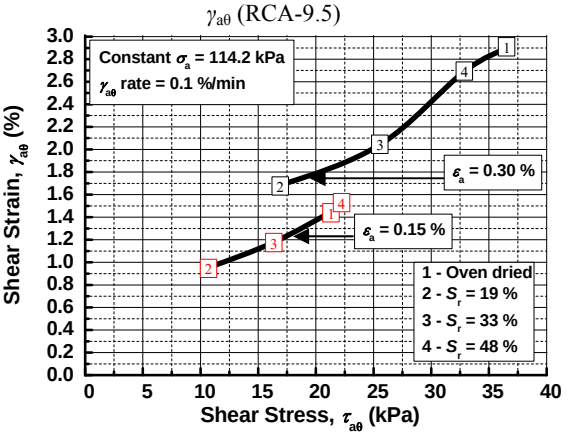

Figure 10 $\tau_{a\theta}$ - $\gamma_{a\theta}$ relationships during static shearing test at the same ε_a (RCA-9.5)

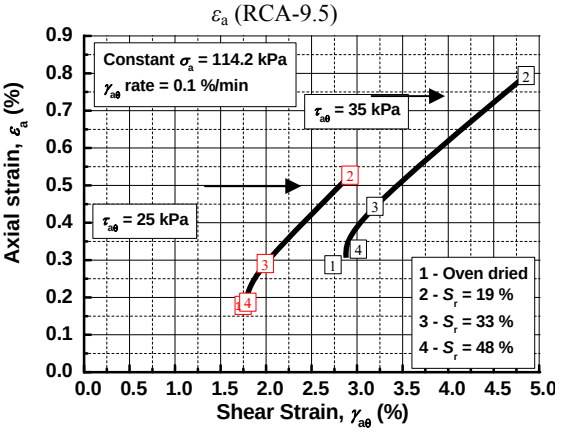

Figure 11 $\gamma_{a\theta}$ - ε_a relationships during static shearing test at the same $\tau_{a\theta}$ (RCA-9.5)

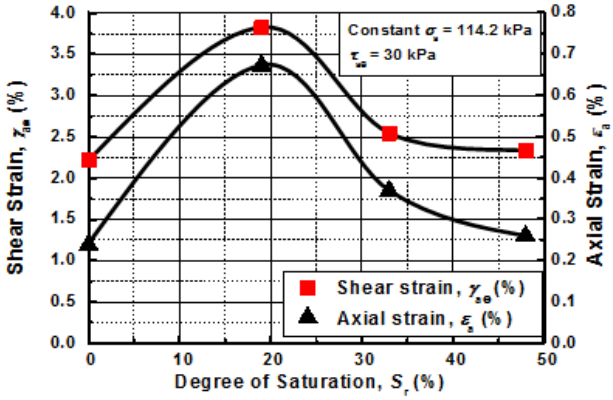

Figure 12 S_r - $\gamma_{a\theta}$ and S_r - ε_a relationships under static shearing test (RCA-9.5)

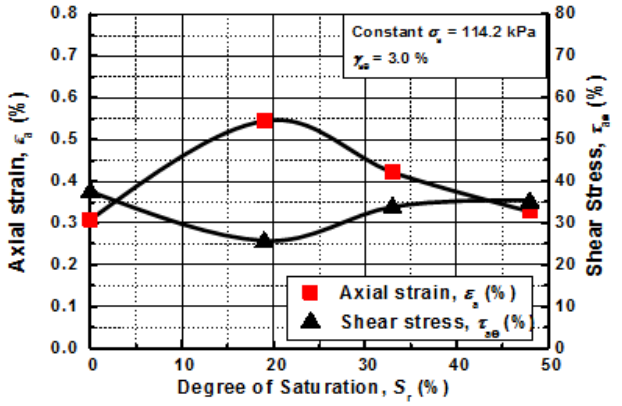

Figure 13 S_r - ε_a and S_r - $\tau_{a\theta}$ relationships under static shearing test (RCA-9.5)

4.2 Influence of matric suction on shear behavior

In order to understand the dependency of the shear behavior of RCA-9.5 material on s, the shear strength equations for unsaturated soils, as mentioned in Equations 1 to 3 are analyzed.

$$\sigma' = (\sigma_a - u_a) + \chi(u_a - u_w)$$
(Bishop's equation for unsaturated soils) (1)

$$\chi = (S_r - S_{r0}) / (1 - S_{r0})$$
(Vanapalli and Fredlund 1999 and Lu and Likos 2004) (2)

$$\tau = c' + \sigma' \tan\phi'$$ (Coulomb's equation) (3)

Where τ: shear stress, c': effective cohesion, σ': effective normal stress, $(\sigma_a - u_a) = \sigma_{n(net)}$: net normal stress, ϕ': effective internal friction angle, $(u_a - u_w) = s$: matric suction, χ: parameter related to the degree of saturation of the soil, S_r: degree of saturation at any s, S_{r0}: residual degree of saturation.

It is explained that the air-water interface in the unsaturated soil is termed as contractile skin which possesses a property called surface tension (Fredlund and Rahardjo 1993). As a result of surface tension in the contractile skin, the capillary effect appears in the unsaturated soil. It is found that due to the capillary effect, the water pressure in the capillary height is negative and the air pressure is atmospheric, which constitute s. The second part of Bishop's equation for the unsaturated soils (Equation 1) illustrates the suction stress $\chi(s)$, which is mainly dependent on the S_r and the s value. It is pertinent to mention here that χ is not only a function of S_r but also a function of the air-entry value. However, as described in this research that s at air-entry value for the SWCC of C-9.5 and RCA-9.5 materials could not be clearly recognized / noticed and thus will not influence the χ. Therefore in this research χ is mainly related to the S_r of the soil. Bishop's equation for the unsaturated soils (Equation 1) describes the effect of $\chi(s)$ on the σ'. In the light of equations 1 and 3, due to increase in $\chi(s)$, the σ' increases and, as a result, the τ increases under keeping constant $\sigma_{n(net)}$ and c'. The s values were obtained from the soil water characteristic curve, in which the ρ_{dc} of 1.470 g/cm^3 was maintained throughout the water retentivity test as shown in Figure 4. During the multi-ring shear tests on the unsaturated RCA-9.5 material, the u_a thought to remains at atmospheric pressure, while the u_w becomes negative as shown in Figure 4. In case of the static shearing test, the ρ_d after static shearing test at the $\gamma_{a\theta}$ of 3.0 %, slightly increases due to small increase in ε_a, as shown in Figure 13. Based on the small ε_a occurrence, and as a result of the slight increase in ρ_d, the s values obtained from the soil water characteristic curve shown in Figure 4 are considered appropriate to evaluate the influence of s on the shear behavior of the RCA-9.5 material. The oven dried sample does not contain water content; therefore, $\chi(s)$ is not applicable in the case of oven dried sample. Whereas, in case of S_r = 19 %, the S_r is less than the S_{r0} as shown in Figure 4. It is difficult to determine s values for coarse grained material at S_r less than S_{r0} on the SWCC obtained from water retentivity test carried out on triaxial apparatus. Therefore, in this research the s value for S_r = 19 % cannot be evaluated. Whereas, samples with S_r = 33 % and 48 % have the χ values about 0.10 and 0.30 according to equation 2 and the s values about 2.0 kPa and 1.25 kPa as shown in drying curve of Figure 4 respectively. Therefore, in this research the s of samples with S_r = 33 % and 48 % after multiplying with their χ parameter has an insignificant influence on the shear behavior of RCA-9.5 material because the capillary effect in RCA-9.5 material is not much dominant to develop the $\chi(s)$.

4.3 Shear behaviour comparison between RCA-9.5 and C-9.5

In Figure 5, the $\tau_{a\theta}$ distribution indicates that the maximum shear stress $\tau_{a\theta max}$ occurs at ±30 kPa and the σ_{amax} takes place at 114.2 kPa therefore, influence of the S_r on the ε_a and the $\gamma_{a\theta}$ behavior of the RCA-9.5 and C-9.5 materials under the static shearing test is compared at the $\tau_{a\theta}$ of 30 kPa and the constant σ_a of 114.2 kPa, as shown in Figures 14 and 15. The results of C-9.5 material were taken from previous research (Inam et al. 2012). Figures 14 and 15 exhibit that the ε_a and the $\gamma_{a\theta}$ for the C-9.5 material at the $\tau_{a\theta}$ of 30 kPa are lesser than the RCA-9.5 material under the same S_r. It is also shown that oven dried sample has the ε_{amin} and the $\gamma_{a\theta min}$ under each material; C-9.5 and RCA-9.5. This reveals that the oven-dried sample has the strongest resistance against the shear loading. Subsequently, with increase of the water content up to S_r = 19 %, the ε_a and the $\gamma_{a\theta}$ increases significantly and reaches the maximum deformation value for each curve and thus resulting the weakest resistance against the shear loading. With further increase of the water content up to S_r = 33 %, the ε_a and the $\gamma_{a\theta}$ decreases. Finally when water content is added up to S_r = 48 %, the ε_a and the $\gamma_{a\theta}$ further decreases for the RCA-9.5 and C-9.5 materials.

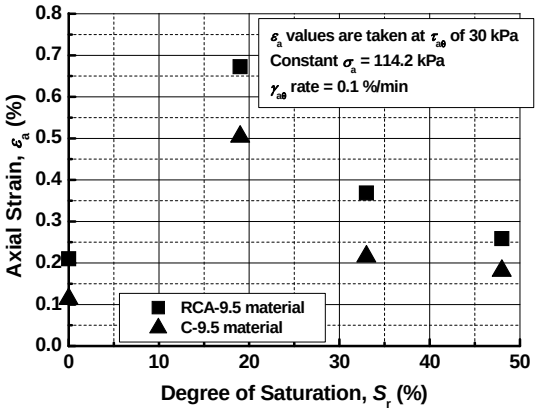

Figure 14 S_r - ε_a relationships under static shearing test

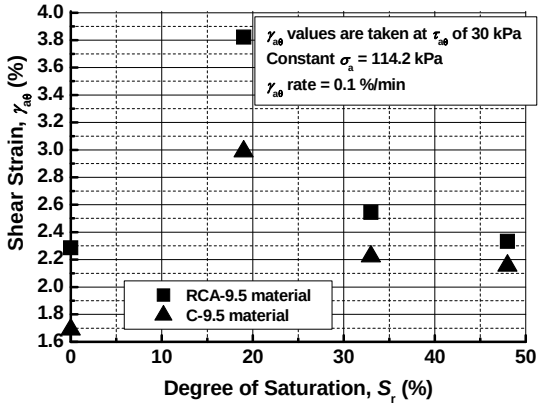

Figure 15 S_r - $\gamma_{a\theta}$ relationships under static shearing test

4.4 Deformation behavior under cyclic loading

In the case of a pavement analysis, permanent axial strain ε_a^p is an important factor in assessing failure or deterioration of pavements. Lekarp et al. (1996) defined that granular materials exhibit two types of deformation, when subjected to repeated loading: resilient deformation which could lead to fatigue cracking of the asphalt surface, and the permanent (plastic) deformation, which may lead to rutting. The permanent deformation during one cycle of loading is normally just a fraction of the total deformation produced by each load repetition. Though, the gradual accumulation of a large number of these small plastic deformation increments could lead to an eventual failure of the pavement due to excessive rutting (Lekarp and Dawson 1998). Therefore, it is valuable to analyze the cyclic plastic deformation behavior of the RCA-9.5 material with and without principal stress axis rotation under different S_r. Here, ε_a^p represents the cumulative permanent axial strain. The outcomes of cyclic loading tests; repeated axial loading and repeated axial and shear loading with $\tau_{a\theta max}$ = 30 kPa are presented in Figures 16 and 17 respectively for the RCA-9.5 material in the form of cumulative permanent axial strain under different number of loading cycles N_c and S_r. Figures 16 and 17 show that, with an increasing N_c, the permanent deformation increases considerably during the initial loading cycles. However, during later cycles, the permanent deformation curves become relatively flatter regardless of the S_r.

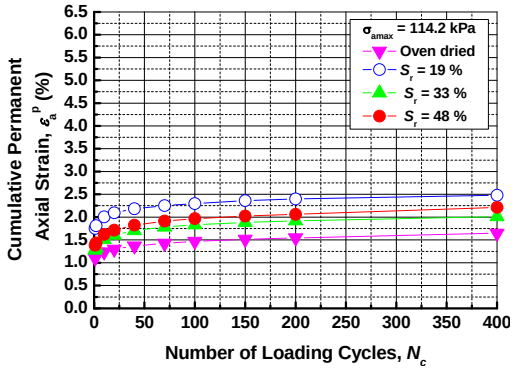

Figure 16 Permanent deformation during repeated axial loading tests (RCA-9.5)

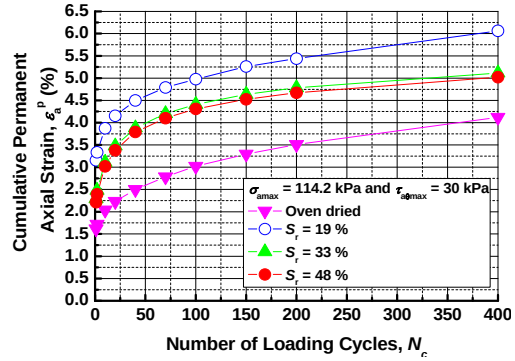

Figure 17 Permanent deformation during repeated axial and shear loading tests (RCA-9.5)

4.5 Influence of degree of saturation on deformation behavior

The permanent axial deformation of the RCA-9.5 material may be influenced by several factors, namely, physical characteristics such as particle size distribution, the density achieved before application of loading, the magnitude & type of loading and the S_r.

The particle size distribution of the RCA-9.5 material is examined before and after each test and there is no breakage of particles or changes in the particle size distribution regardless of the S_r. The same dry densities were taken for all the specimens before the cyclic loading tests and same magnitude of loading for each type is applied as mentioned in Table 3. Accordingly, as shown in Figures 16 and 17, when comparing the ε_a^p under each cyclic loading condition, the S_r is the only variable which influences the cyclic plastic deformation behavior of the RCA-9.5 material under same N_c.

Figure 18 shows ε_a behavior of unsaturated specimens under different types of loading methods. The influence of S_r on ε_a^p behavior for repeated axial loading and repeated axial and shear loading tests is evaluated at 400th number of loading cycle. Figure 18 shows that the oven-dried sample under repeated axial loading test has a minimum cumulative permanent axial strain $\varepsilon_a^p{}_{min}$. This reveals that the oven-dried sample has the slightest change in height and accordingly minimum rearrangement of the particles occurs. Subsequently, the increase in water content causes an increase in the ε_a^p till S_r reaches at 19 % and, as a result, settlement of particles also increases. With the further increase of S_r up to 48 %, ε_a^p drops and the deformation of sample decreases.

In Figure 18, when comparing the ε_a^p of unsaturated samples under repeated axial and shear loading test, it is found again that oven-dried sample has a $\varepsilon_a^p{}_{min}$ and thus resulting in the least change in height of specimen. Figure 18 shows that with the increase of water content, up to S_r = 19 %, the ε_a^p increases significantly and reaches the maximum cumulative permanent axial strain $\varepsilon_a^p{}_{max}$. With the further increase of water content, up to S_r = 48 %, the ε_a^p decreases and accordingly the settlement of sample decreases.

In the static shearing test similar trend was observed as mentioned above and shows that the maximum axial deformation occurs at S_r = 19 %. The above discussion elucidates that the influence of S_r on the deformation behavior has some similarity for all loading methods but the differences are in the magnitude of deformation under various loading methods. The difference in the magnitude of deformation is further explained in latter sections.

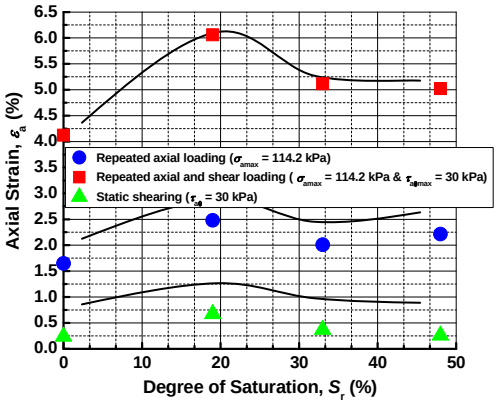

Figure 18 S_r - ε_a relationships (RCA-9.5)

4.6 Calculation of rotational angle of principal stress axis

The rotational angle of principal stress axis ω is calculated to evaluate the general stress condition of the RCA-9.5 material due to the repeated axial and shear loading test. The ω, major principal stress σ_1, intermediate principal stress σ_2, and minor principal stress σ_3, can be calculated with the following equations.

$$\omega = \sin^{-1} \{(\sigma_2 - \sigma_3) / (\sigma_1 - \sigma_3)\}^{1/2}$$
Rotational angle of principal stress axis (4)

$$\sigma_1 = (\sigma_a + K_0\,\sigma_a)/2 + [\{(\sigma_a - K_0\,\sigma_a)^2 + 4\,\tau_{a\theta}{}^2\}^{1/2}]/2$$
Major principal stress (5)

$$\sigma_2 = \sigma_r = K_0\,\sigma_a$$
Intermediate principal stress (6)

$$\sigma_3 = (\sigma_a + K_0\,\sigma_a)/2 - [\{(\sigma_a - K_0\,\sigma_a)^2 + 4\,\tau_{a\theta}{}^2\}^{1/2}]/2$$
Minor principal stress (7)

The principal stresses and the ω have been calculated by inserting values of the K_0, the cyclic σ_a and the cyclic $\tau_{a\theta}$ into Equations 4 to 7. During cyclic loading tests, the K_0 may change with the N_c for each test. In this research, lateral stress σ_r was not measure. For this reason the K_0 is assumed to be constant throughout the test. Ishikawa et al. (2011) has taken the K_0 values from 0.2 to 0.4 for describing the relationship of the maximum rotational angle of principal stress axis ω_{max} and the $\tau_{a\theta}$ amplitude by using the coarse granular material (Angular, crushed hard andesite stone with maximum particle size of about 12 mm) employed in the rail-road ballast. There are few research works that describe about the estimation method of the K_0 for the recycled coarse granular material. Keeping in view the above explanation, the wide range of K_0 values from 0.2 to 0.4 is considered in this research for the calculation purpose of ω, therefore; the purpose of this calculation is to analyze the occurrence of ω due to repeated axial and shear loading test under different K_0 values. The other purpose is to evaluate the effect of $\tau_{a\theta}$ amplitudes on the ω_{max} under different K_0 values for the same cyclic σ_a values.

Figure 19 shows that change in ω during a loading cycle of repeated axial and shear loading test under different K_0 values. The ω increases cyclically and reaches the highest value at a certain combination of the σ_a and the $\tau_{a\theta}$. In other words, the ω_{max} is mainly dependent on the loading condition of the multi-ring shear tests. The graph also elucidates that the ω_{max} for repeated axial and shear loading tests under different K_0 values occurs after the same interval of time. The sign of ω changes continuously from positive to negative as the $\tau_{a\theta}$ cyclically changes from positive to negative and vice versa. In Figure 20 the relationships between $\tau_{a\theta}$ amplitude and the ω_{max} at different K_0 values under the same σ_a amplitude are elaborated. It shows that the higher the $\tau_{a\theta}$ amplitude is, the larger the ω_{max} becomes under a constant K_0. Similarly, the higher the K_0 is, the larger the ω_{max} becomes under constant $\tau_{a\theta}$ amplitude. The results explain that the variation in ω_{max} due to change in K_0 from 0.20 to 0.40 at the same $\tau_{a\theta}$ amplitude is smaller compared to the variation in ω_{max} due to the change in $\tau_{a\theta}$ amplitude from 15 kPa to 30 kPa under same K_0.

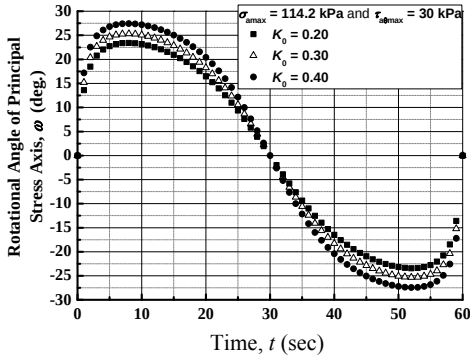

Figure 19 Rotational angle of principal stress axis under repeated axial and shear loading tests

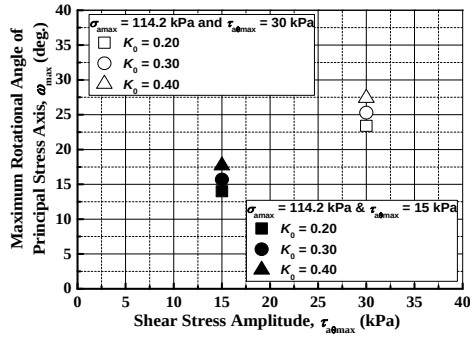

Figure 20 $\tau_{a\theta max}$ - ω_{max} relationships under repeated axial and shear loading tests

4.7 Influence of rotational angle of principal stress axis on cyclic plastic deformation behavior

Figure 21 shows the example of relationships between the p and the ω during cyclic loading tests at K_0 = 0.30. During a loading cycle, the p under each loading method has same value at the same interval of time. However, the ω during a loading cycle varies by the difference in loading method at the same interval of time. One point must be kept in mind, namely, that the loading cycle of σ_a is same for both types of cyclic loading tests employed in this research, but only the $\tau_{a\theta}$ amplitude changes in the cyclic loading tests. Therefore, due to the shift from repeated axial loading test to repeated axial and shear loading test, the major and the minor principal stresses also vary due to the change in the $\tau_{a\theta}$ amplitude at the same K_0 value.

It is found that when the $\tau_{a\theta}$ amplitude increases from 0 kPa to 30 kPa, increase in the major principal stresses occur equally to the decrease in the minor principal stresses and that no deviation occurs in the intermediate principal stresses during a loading cycle at the same K_0 value. This reveals that the mean principal stresses remain the same for both loading methods under the same K_0. However, deviations in the major and the minor principal stresses due to the increase in $\tau_{a\theta}$ amplitude, cause difference in the ω. It is also indicated in Figure 21 that when the $\tau_{a\theta}$ amplitude increases to 30 kPa, the ω also increases under the same p. Therefore, the difference in ε_a^p between the repeated axial loading test and the repeated axial and shear loading test under the same experimental conditions as shown in Figure 18, is mainly influenced by changes in the ω.

In this research, an attempt is also made to analyze the effect of the ω_{max} on the ε_a^p obtained under both types of cyclic loading tests at 400th N_c for the RCA-9.5 material. The K_0 value is taken as 0.30 for the analysis purpose. Figure 22 shows that the ω_{max} depends on the $\tau_{a\theta}$ amplitude to influence the ε_a^p values of the RCA-9.5 material. It is observed that, the ω_{max} increases with the increase in the $\tau_{a\theta}$ amplitude, and as a result the ε_a^p also increases under the same cyclic σ_a, S_r and K_o value.

Keeping in view the above, the enhancement of ε_a^p due to shift of repeated axial loading to repeated axial and shear loading test, as shown in Figure 18 is mainly influenced by the rotation of the principal stress axis irrespective of the S_r. The impact of the enhanced ε_a^p has been discussed by many researchers. It has been found that under the same cyclic σ_a, the rotation of the principal stress axis occurs mainly due to the application of $\tau_{a\theta}$, and thus, causes an increase in the axial deformation. Ishikawa et al. (2011) compared the cyclic plastic deformation of multi-ring shear tests under cyclic loading with or without principal stress axis rotation to the results of small scale model tests. The results of the small-scale model tests indicated similarity in the enhanced behavior of the cyclic plastic deformation in repeated axial and shear loading test with multi-ring shear testing and examined the validity of multi-ring shear test results. Moreover, in previous research on C-9.5 material (Inam et al. 2012), similar trend was seen that ε_a^p was enhanced due to the principal stress axis rotation. Therefore, the enhanced deformation due to the principal stress axis rotation is considered more reliable for pavement analysis, as it is closer to the phenomenon under traffic loads.

In this research, the cyclic plastic deformation behavior of C-9.5 and RCA-9.5 material with S_r = 19 % is compared under repeated axial loading and repeated axial and shear loading tests in order to analyze the effect of the principal stress axis rotation. These samples are selected as the $\varepsilon_a^p{}_{max}$ occurs at S_r = 19 % under each loading method for the RCA-9.5 material. In Figure 23, results show that the slope of the curves from 200 to 400 N_c for the repeated axial loading test is milder, as compared to the slope of the curves for the repeated axial and shear loading. It is also noted that with provision of the principal stress axis rotation as in the case of repeated axial and shear loading, stability in the particles decreases, thus, causes steeper slope, and as a result, the ε_a^p increases. Therefore, the cyclic loading without principal stress axis rotation as in the case of

repeated axial loading shows that the slope of the curves becomes flatter and showing more stabilization among particles, and as a result, the ε_a^p decreases. When the difference in the ε_a^p of C-9.5 and RCA-9.5 is compared from 0 to 400 N_c under identical cyclic loading method, Figure 23 illustrate that the difference in the ε_a^p between C-9.5 and RCA-9.5 mainly contributes by the initial loading cycles.

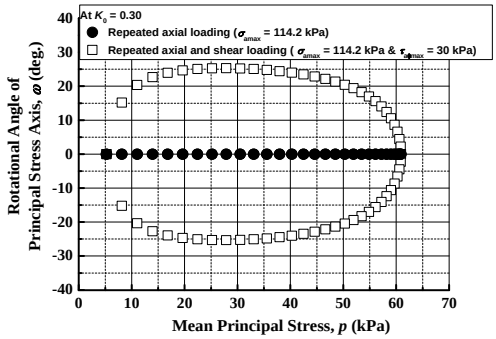

Figure 21 p - ω relationships during a loading cycle of cyclic loading tests

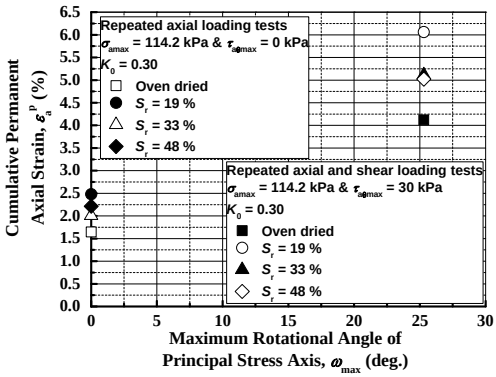

Figure 22 ω_{max} - $\varepsilon_a^p{}_{max}$ relationships under repeated axial and shear loading tests (RCA-9.5)

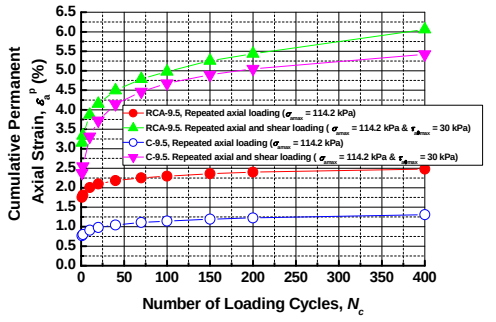

Figure 23 Permanent deformation during cyclic loading at S_r =19 %

4.8 Comparison of deformation behavior between RCA-9.5 and C-9.5

The influence of S_r on the ε_a^p under cyclic loading tests for C-9.5 and RCA-9.5 materials as shown in Figures 24 and 25 is compared at the 400th N_c. Note that results of C-9.5 material in this research under repeated axial loading tests vary from previous research (Inam et al. 2012) because this research includes new test results obtained from the multi-ring shear tests under the same experimental conditions as in the previous research. Figures 24 and 25 clearly indicate that the ε_a^p for C-9.5 material at the 400th N_c under same S_r are lesser than the ε_a^p for RCA-9.5 material. In this research, the results of static shearing tests also indicate that the axial deformation for C-9.5 material is lesser than the axial deformation for RCA-9.5 material under same S_r. These results exhibits that C-9.5 material has more strength to resist cyclic loading compared to RCA-9.5 material and, as consequence, the less ε_a^p occurs for C-9.5 material under same experimental conditions. These results are in line with the physical properties of the test materials as shown in Table 1. The recycled crusher-run material has the higher abrasion value compared to the natural crusher-run material. The strength of the recycled crusher-run material to resist the cyclic loading is lesser when compared with the natural crusher-run material. Therefore, relationship can be obtained that the higher the abrasion value the lesser will be the strength to resist cyclic loading. A recycled material obtained from the demolished concrete structure has hydrated cement that reduces the specific gravity G_s of material and increase the water absorption (Kobayashi and Kawano 1988). The higher the water absorption, the weaker generally is the base course material, and as a consequence, the strength of a recycled material to resist the cyclic loading decreases compared to natural material.

It is also shown in the Figures 24 and 25 that the oven dried sample has the $\varepsilon_a^p{}_{min}$ for both materials; C-9.5 and RCA-9.5 under both cyclic loading tests. This reveals that an oven-dried sample has the strongest resistance against cyclic loading. Moreover, the influence of water on the C-9.5 and RCA-9.5 materials increases the ε_a^p, when compared with the oven-dried samples of C-9.5 and RCA-9.5 materials respectively under each cyclic loading method.

In highway design guides, the S_r at w_{opt} for the base course is generally taken into consideration for the design and analysis of the pavement because the w_{opt} is applied on the base course during the construction of roads in order to achieve ρ_{dmax}. After the construction, the S_r inside base course generally varies due to the infiltration and seasonal variation of ground water level. As described in the example of Tomakomai field measurement site (Ishikawa et al. 2012a) that at the most of the time in a year, the S_r inside real sub-base course is more corresponding to S_{r0}. Thus, it is important to compare the ε_a^p of RCA-9.5 and C-9.5 materials at the S_{r0} under cyclic loading tests. The Figures 24 and 25 clearly point out that ε_a^p has a lesser value at the S_{r0} of C-9.5 material, when compared with the S_{r0} of RCA-9.5 material under both types of cyclic loadings. On the basis of explanation in this research, the phenomenon of the principal stress axis rotation produced under traffic load is better expressed by repeated axial and shear loading test and, therefore, the deformation behavior under repeated axial and shear loading test is much more reliable and realistic. In Figure 25, the difference between the ε_a^p for RCA-9.5 material at the S_{r0} and C-9.5 material at the S_{r0} is much larger than the difference between the ε_a^p for RCA-9.5 and C-9.5 materials under the same S_r during repeated axial and shear loading tests. As a consequence, in real conditions, the mechanical behavior in terms of the cyclic plastic deformation of RCA-9.5 material may be significantly influenced by traffic loading, when compared with the mechanical behavior of C-9.5 material.

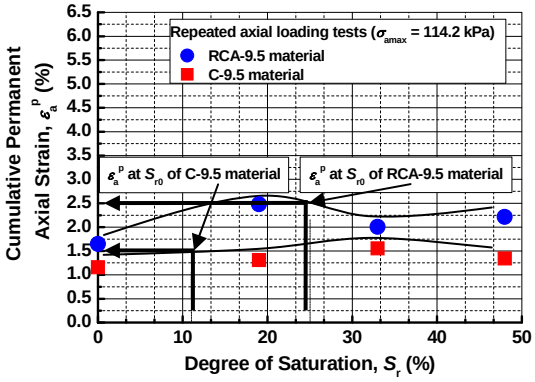

Figure 24 S_r - ε_a^p relationships under repeated axial loading test

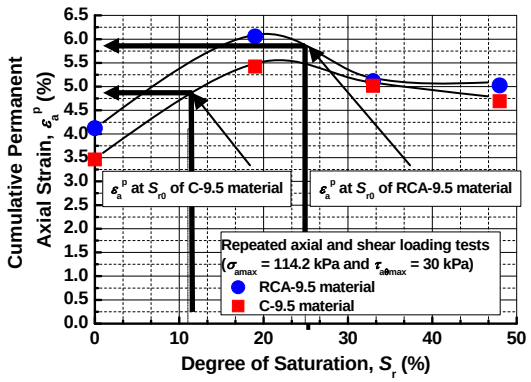

Figure 25 S_r - ε_a^p relationships under repeated axial and shear loading test

5. CONCLUSION

On the basis of above experimental results and discussions, the following conclusions can be obtained.

1) The matric suction s value for the unsaturated RCA-9.5 material has an insignificant influence on the shear behavior because the SWCCs of RCA-9.5 and C-9.5 materials indicate low matric suction values.
2) The influence of the S_r on the shear behavior of C-9.5 material and RCA-9.5 material has similar trend under the same experimental conditions. The static shearing test results of both materials show that the oven-dried sample with S_r = 0 % has the strongest resistance and sample with S_r = 19 % has the weakest resistance against shearing. The results further explain that RCA-9.5 has the higher ε_a and $\gamma_{a\theta}$ values under the same $\tau_{a\theta}$ when compared with the C-9.5 material at each S_r.
3) The C-9.5 material has the lesser ε_a^p, when compared with the RCA-9.5 material under each cyclic loading method and at the same S_r. This behavior confirms that the RCA-9.5 material is weaker to resist the cyclic loading, when compared with the C-9.5 material. The physical properties such as the water absorption and the abrasion value also validate the results.
4) It is found that at the S_{r0} of RCA-9.5 and C-9.5 materials, the ε_a^p for C-9.5 material is lesser than that of RCA-9.5 material under each cyclic loading method. During repeated axial and shear loading the ε_a^p for C-9.5 material at the S_{r0} is significantly lesser than that of RCA-9.5 material at the S_{r0}, when comparing the difference in ε_a^p between RCA-9.5 and C-9.5 materials under the same S_r. This indicates that in the real conditions, the permanent deformation of RCA-9.5 material at the S_{r0} can be considerably increased when compared with the C-9.5 material at the S_{r0}.
5) The deformation behavior of the unsaturated RCA-9.5 and C-9.5 materials under each cyclic loading method indicates that the ε_a^p varies due to the influence of S_r. It is also observed that for the RCA-9.5 and C-9.5 materials, increase in the ε_a^p takes place due to the shift of the repeated axial loading test to the repeated axial and shear loading test. Hence, the influence of the principal stress axis rotation on RCA-9.5 material shows the similar enhanced behavior of the ε_a^p as it was found in the C-9.5 material (Inam et al. 2012) under the same experimental conditions. The difference in the ε_a^p between RCA-9.5 and C-9.5 materials occurs subject to the influence of S_r and type of material.

In the pavement design and analysis, the behavior under S_r at the w_{opt} for the base course is generally considered. However, the behavior under S_{r0} of the base course can also be taken into account along with that under S_r at the w_{opt} for the pavement design and analysis. It is very important to compare the mechanical behavior in terms of cyclic plastic deformation of the natural and recycled base course materials at the corresponding S_{r0} in order to correctly incorporate the effect of cyclic plastic deformation behavior of the recycled material in the designing of pavement. However, the above conclusions are based on some limited testing conditions and analysis. There is a room for further research to investigate recycled material from other sources in order to establish representativeness of recycled sample used in this research.

6. ACKNOWLEDGEMENT

The authors express their deepest gratitude to Hirosato Segawa, Master Course Student Hokkaido University, who performed water retentivity test and arranged the experimental results.

7. REFERENCES

AASHTO T 307-99 (2007), (2009) “Standard test method for determining the resilient modulus of soils and aggregate materials”, Standard Specifications for Transportation Materials and Methods of Sampling and Testing, 29th Edition.

ASTM designation 6836-02 (2010) “Standard test method for determination of the soil water characteristic curve for desorption using a hanging column, pressure extractor, chilled mirror hygrometer, and/or centrifuge”, ASTM Volume 04.09.

Brown, S. F. (1996) “Soil mechanics in pavement engineering”, Géotechnique, 46(3), pp383-426.

Chan, F. W . K. and Brown, S. F. (1994) “Significance of principal stress rotation in pavements”, Proceedings of 13th Int. Conference on Soil Mechanics and Foundation Engineering, New Delhi, pp1823-1826.

Ekblad, J. and Isacsson, U. (2006) “Influence of water on resilient properties of coarse granular materials”, Road Material and Pavement Design, 7(3), pp369-404

Fredlund, D. G. and Rahardjo, H. (1993) “Soil mechanics for unsaturated soil”, New York: John Wiley & Sons.

Fredlund, D. G. and Xing, A. (1994) “Equations for the soil water characteristic curves”, Canadian Geotechnical Journal, 31(4), pp521-532.

Gräbe, P. J. and Clayton, C. R. I. (2009) “Effects of principal stress rotation on permanent deformation in rail track foundations”, Journal of Geotechnical and Geoenvironmental Engineering, 135(4), pp555-565.

Gabr, A. and Cameron, D. (2012) “Properties of recycled concrete aggregate for unbound pavement construction”, Journal of materials in Civil Engineering, 24(6), pp754-764.

Ishikawa, T., Miura, S. and Sekine, E. (2007) “Development and performance evaluation of multi-ring shear apparatus”, Proceedings of Int. Workshop on Geotechnical Aspects and Processed Material, Osaka, 13th September 2005, pp53-64.

Ishikawa, T., Tokoro, T., Ito, K. and Miura, S. (2010) “Testing methods for hydro-mechanical characteristics of unsaturated soils subjected to one-dimensional freeze-thaw action”, Journal of Soils and Foundations, 50(3), pp431-440.

Ishikawa, T., Sekine, E. and Miura, S. (2011) “Cyclic deformation of granular material subjected to moving-wheel loads”, Canadian Geotechnical Journal, 48(5), pp691-703.

Ishikawa, T., Kawabata, S., Kameyama, S., Abe, R. and Ono, T. (2012a) “Effects of freeze-thawing on mechanical behavior of granular base in cold regions”, Proceedings of 2nd Int. Conference on Transportation Geotechnics, Sapporo, 10-12 September 2012, pp118-124.

Ishikawa, T., Zhang, Y., Segawa, H. and Miura, S. (2012b) “Development of medium-size triaxial apparatus for unsaturated granular base course materials”, Proceedings of 2nd Int. Conference on Transportation Geotechnics, Sapporo, 10-12 September 2012, pp534-540.

Inam, A., Ishikawa, T. and Miura, S. (2012) "Effect of principal stress axis rotation on cyclic plastic deformation characteristics of unsaturated base course material", Journal of Soils and Foundations, 52(3), pp465-480.

Japan Road Association (1989): "Manual for asphalt pavement," Japan Road Association.

Japan Road Association (2006): "Pavement design manual," Tokyo: Japan Road Association. (in Japanese).

Japan Standards Association (2009) "Test method for soil compaction using a rammer (JIS A 1210: 2009)", Japanese Industrial Standards. (in Japanese)

Japan Geotechnical Society (2009) "Test method for water retentivity of soils (JGS 0151-2009)", Japanese Geotechnical Society. (in Japanese)

Kobayashi, S. and Kawano, H. (1988) "Properties and usage of recycled aggregate concrete", Proceedings of 2nd Int. Symposium on Reuse of Demolition Waste, Tokyo, Japan, 7-11 November 1988.

Lekarp, F., Richardson, I. R. and Dawson, A. (1996) "Influence on permanent deformation behavior of unbound granular materials", Transportation Research Record, 1547(1), pp68-75.

Lekarp, F. and Dawson, A. (1998) "Modeling permanent deformation behavior of unbound granular material", Construction and building materials, 12(1), pp9-18.

Lu, N. and Likos, W. J. (2004) "Unsaturated soil mechanics", New Jersey: John Wiley and Sons Inc, Hoboken.

Poon, C. S. and Chan, D. (2006) "Feasible use of recycled concrete aggregates and crushed clay brick as unbound road sub-base." Construction and building baterials, 20(8), pp578-585.

Rahardjo, H., Vilayvong, K. and Leong, E. C. (2011) "Water characteristic curves of recycled material", Geotechnical Testing Journal, 34(1).

Vanapalli, S. K., Sillers, W. S. and Fredlund, M. D. (1998) "The meaning and relevance of residual state to unsaturated soils", Proceedings of the 51st Canadian Geotechnical Conference, Edmonton, Alberta, 4-7 October 1998.

Vanapalli, S. K. and Fredlund, D. G. (1999) "Empirical procedures to predict the shear strength of unsaturated soils", Proceedings of the 11th Asian Regional Conference on Soil Mechanics and Geotechnical Engineering, Seoul, 16-20 August 1999, pp93-96.